BIOCHEMISTRY
including biophysical chemistry & molecular biology

Article

pubs.acs.org/biochemistry

A Dimeric Chlorite Dismutase Exhibits O_2-Generating Activity and Acts as a Chlorite Antioxidant in *Klebsiella pneumoniae* MGH 78578

Arianna I. Celis,[†] Zachary Geeraerts,[‡] David Ngmenterebo,[§] Melodie M. Machovina,[†] Richard C. Kurker,[∥] Kumar Rajakumar,[§] Anabella Ivancich,[⊥] Kenton R. Rodgers,[‡] Gudrun S. Lukat-Rodgers,*[,‡] and Jennifer L. DuBois*[,†]

[†]Department of Chemistry and Biochemistry, Montana State University, Bozeman, Montana 59715, United States

[‡]Department of Chemistry and Biochemistry, North Dakota State University, Fargo, North Dakota 58102, United States

[§]Department of Chemistry and Biochemistry, University of Notre Dame, Notre Dame, Indiana 46556, United States

[∥]Department of Infection, Immunity and Inflammation, University of Leicester, Leicester LE1 9HN, U.K.

[⊥]CNRS, Unité de Recherche Mixte CNRS/CEA/Université Paris-Sud (UMR 8221), Laboratoire de Bioénergétique, Métalloprotéines et Stress, Centre d'Etudes de Saclay, iBiTec-S, 91191 Gif-sur-Yvette, France

Supporting Information

ABSTRACT: Chlorite dismutases (Clds) convert chlorite to O_2 and Cl^-, stabilizing heme in the presence of strong oxidants and forming the O═O bond with high efficiency. The enzyme from the pathogen *Klebsiella pneumoniae* (*Kp*Cld) represents a subfamily of Clds that share most of their active site structure with efficient O_2-producing Clds, even though they have a truncated monomeric structure, exist as a dimer rather than a pentamer, and come from Gram-negative bacteria without a known need to degrade chlorite. We hypothesized that *Kp*Cld, like others in its subfamily, should be able to make O_2 and may serve an *in vivo* antioxidant function. Here, it is demonstrated that it degrades chlorite with limited turnovers relative to the respiratory Clds, in part because of the loss of hypochlorous acid from the active site and destruction of the heme. The observation of hypochlorous acid, the expected leaving group accompanying transfer of an oxygen atom to the ferric heme, is consistent with the more open, solvent-exposed heme environment predicted by spectroscopic measurements and inferred from the crystal structures of related proteins. *Kp*Cld is more susceptible to oxidative degradation under turnover conditions than the well-characterized Clds associated with perchlorate respiration. However, wild-type *K. pneumoniae* has a significant growth advantage in the presence of chlorate relative to a Δ*cld* knockout strain, specifically under nitrate-respiring conditions. This suggests that a physiological function of *Kp*Cld may be detoxification of endogenously produced chlorite.

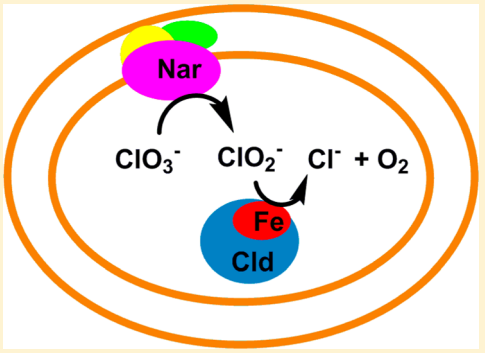

O_2 bond-forming processes are rare in biology. At present, two examples are well-described. First, the water-splitting reaction catalyzed by photosystem II (PSII) drives the photosynthetic fixation of CO_2 into carbohydrates.[1] Second, a much more unusual reaction found in perchlorate (ClO_4^-)-respiring bacteria is used to detoxify chlorite (ClO_2^-), the end product of the perchlorate respiratory pathway. ClO_2^- is rapidly converted to O_2 and Cl^- via an enzyme known as chlorite dismutase (Cld).[2] In sharp contrast with the complexity of PSII,[1] Clds are soluble enzymes catalyzing an O−O bond-forming reaction with heme *b* as the sole cofactor.

Clds from perchlorate-respiring bacteria catalyze this reaction with great efficiency. The enzyme from *Dechloromonas aromatica* (*Da*Cld), which we have characterized extensively and use here as an example of a highly adapted respiratory Cld, turns over >20000 equiv of chlorite per heme at rates nearing the diffusion limit before it is irreversibly inactivated.[3−7] The proposed mechanism for O_2 formation (Scheme 1) involves initial transfer of an oxygen atom from ClO_2^- to the ferric heme

Scheme 1

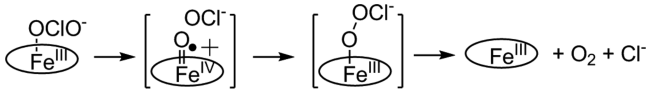

to make an Fe^{IV}═O porphyrin (Por) π-cation radical (Compound I). The resulting hypochlorite (OCl^-) leaving group is stabilized in its nucleophilic, anionic state by a positively charged arginine residue in a sterically confined pocket above the heme plane.[8−11] The "trapped" hypochlorite is then poised for nucleophilic attack on the electron-deficient ferryl oxygen atom to generate a putative ferric peroxyhypochlorite ($OOCl^-$) intermediate that decomposes to yield Cl^- and O_2.

Received: September 19, 2014
Revised: November 26, 2014
Published: December 1, 2014

The requirement for the Cld-catalyzed reaction by perchlorate-respiring bacteria is absolute; without it, ClO_2^- rapidly accumulates to toxic levels.[2] However, Clds are found in almost all bacterial phyla and in many archaea, the overwhelming majority of which are not involved in perchlorate respiration.[12] These Clds subdivide according to sequence into groups that appear to be functionally distinct from their respiration-associated counterparts and from each other (Figure 1), in spite of their high level of sequence similarity.[13] Investigation of the Cld from *Staphylococcus aureus*, a Gram-positive bacterium, provided a striking example. In its heme-bound form, it is completely inactive in the conversion of ClO_2^- to Cl^- and O_2.[14] Genetic and biochemical evidence instead suggests that the protein is essential for a terminal step in heme biosynthesis,[14,15] a biological function that appears to be common to the Clds from Gram-positive bacteria and potentially other species.[13,15]

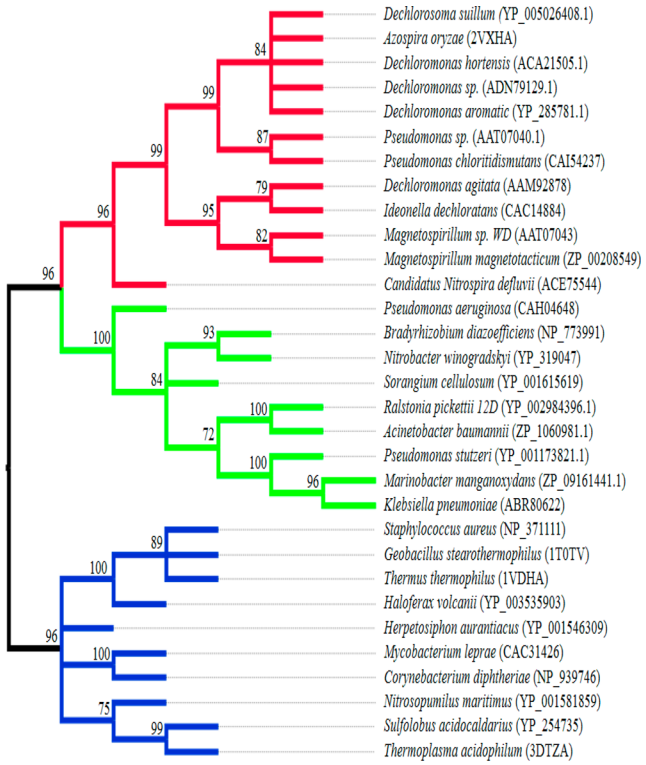

Figure 1. Phylogenetic tree illustrating the major subdivisions of the Cld protein family discussed in the text. The respiratory Clds, coming mostly from Proteobacteria with some exceptions caused by lateral gene transfer, form the first group (red). Members of a second group of dimeric Clds (green), including *Kp*Cld, come from non-perchlorate-respiring species but retain active site features critical for ClO_2^-/O_2 conversion. Members of a third broad group of Clds (blue) catalyze a terminal step in heme biosynthesis in Gram-positive bacteria and potentially some Archaea. These have consequently been renamed HemQs.[11] Sequence accession numbers are given in parentheses, with PDB entries used to indicate where structures are available. The phylogenetic tree was generated using MEGA6.[69] The bootstrap consensus tree inferred from 1000 replicates is taken to represent the evolutionary history of the taxa analyzed. Branches corresponding to partitions reproduced in <70% of bootstrap replicates are collapsed. Initial trees for the heuristic search were obtained by applying the Neighbor-Joining method to a matrix of pairwise distances estimated using a JTT model. A discrete Gamma distribution was used to model evolutionary rate differences among sites [five categories (+*G*, parameter = 2.4895)]; 5% alignment gaps, missing data, and ambiguous bases were allowed at any position.[70] The resulting tree is consistent with those previously reported by others.[11,13,71]

The Cld from *Klebsiella pneumoniae* strain MGH 78578 (*Kp*Cld) represents another subfamily that may have yet a third biochemical function. These enzymes are found in non-perchlorate-respiring bacteria from Gram-negative phyla (Figure 1).[12,13] As a consequence, they are not expected to be involved in either perchlorate respiration or heme biosynthesis. Unlike the respiration-associated Clds, they are homodimers rather than homopentamers, leading to a very different monomer−monomer interface and resulting structural context for their bound hemes (Figure 2A−C). Locally, however, they possess very similar active site residues and share structural attributes essential for efficient ClO_2^-/O_2 conversion. In particular, they share the functionally important distal arginine above the ferric heme's open coordination position (Figure 2D).[8,11] Consistent with chemical expect-

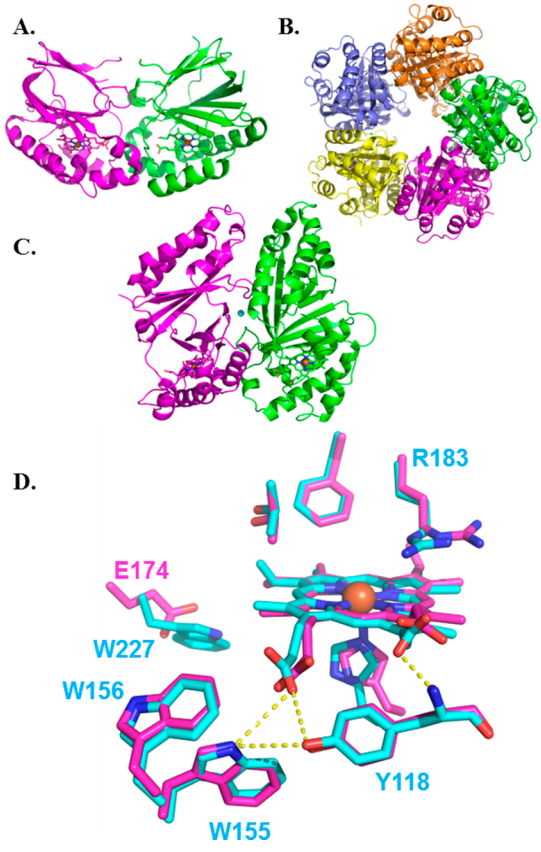

Figure 2. Clds from perchlorate-respiring and nonrespiring Proteobacteria. (A) *Kp*Cld, like the *Nw*Cld structure shown (PDB entry 3QPI),[7] has a truncated monomer relative to the respiratory Clds. Both form functional homodimers. Protein monomers are rendered as cartoons in different colors. Hemes are rendered as sticks. (B) Respiration-associated *Da*Cld (PBD entry 3Q08) forms a functional homopentamer, shown looking down the C_5 axis.[4] (C) A monomer−monomer interface from the structure in panel B suggests differences in heme accessibility in the pentameric and dimeric Clds. (D) Active site environments for *Da*Cld (cyan carbons) and *Nw*Cld (magenta carbons) are superimposed with several conserved residues around the heme labeled (*Da*Cld numbering). The two active sites are highly similar; two notable exceptions are the orientation of the distal Arg side chain and the identity of the residue at the position of W227, which is a conserved glutamate in *Nw*Cld and other dimeric Clds.

dx.doi.org/10.1021/bi501184c | *Biochemistry* 2015, 54, 434−446

ations, O_2 production has been demonstrated for at least one protein from this subgroup, the Cld from *Nitrobacter winogradskyi* [*Nw*Cld (structure shown in Figure 2A,D)];[11] however, the dimeric enzymes have presumably not had the selection pressure to evolve to the same level of efficiency as Clds that are essential for metabolizing perchlorate.

Why bacteria like *K. pneumoniae* MGH 78578, a respiratory pathogen, possess a potential means for chlorite detoxification is not clear. *K. pneumoniae* and other non-perchlorate-respiring species generally do not encode perchlorate or chlorate reductase enzymes,[17] yet pathogenic strains of clinically pervasive[18] species, including *K. pneumoniae*, *Acinetobacter baumanii*, and *Pseudomonas aeruginosa*, all possess genes from this *cld* subtype, often on plasmids or as part of pathogenicity islands. These genes appear unlikely to guard against environmental chlorite, because of its chemical instability and the inability of negatively charged chlorite to passively enter cells.[19] However, an indirect antioxidant function against ClO_3^- or ClO_4^- is possible, if these can enter the cell and be reduced by endogenous enzymes. To test this hypothesis, and to enhance our understanding of the influence of the unusual monomer and oligomerization states on an otherwise similar heme environment, *Kp*Cld was characterized in parallel with the Δ*cld* strain of *K. pneumoniae* MGH 78578. The results presented here report on both the biological function of this group of Clds and the biochemical properties that make them unique.

EXPERIMENTAL PROCEDURES

Chemicals. Chemicals were purchased from Alfa Aesar, Sigma-Aldrich, or VWR. Sodium chlorite, 2,2′-azino-bis(3-ethylbenzothiazoline-6-sulfonic acid) diammonium salt (ABTS), guaiacol, and 2-chloro-5,5-dimethyl-1,3-cyclohexanedione (MCD) stock solutions were made fresh daily in buffers prepared from distilled and deionized water and their concentrations determined spectrophotometrically: ε_{262} = 160 M^{-1} cm^{-1} ($NaClO_2$), ε_{415} = 3.6 × 10^4 M^{-1} cm^{-1} (ABTS), and ε_{290} = 20100 M^{-1} cm^{-1} (MCD).[20] Iodometric titration was routinely used to quantify working solutions of sodium chlorite or hypochlorite [diluted from a 10−14% (w/w) stock], as well as unreacted chlorite remaining at the end of experiments.[21] Each substrate was dissolved directly in the specified aqueous buffers with the exception of guaiacol, for which a 0.9 M stock was prepared in dimethyl sulfoxide (DMSO). Stocks of hemin were prepared in DMSO.

Generation of the Δ*cld* Strain. Mutagenesis of *K. pneumoniae* MGH 78578 was conducted as described previously.[22] Briefly, a derivative of pKOBEG encoding apramycin resistance, pKOBEGApra, was used to facilitate lambda Red-based replacement of *cld* with a 1652 bp FRT site-flanked hygromycin resistance cassette (FRT-*hph*-FRT) amplified from pJTAG-hyg (Deenathayalagaptha and Rajakumar, unpublished data) using primers GmF and GmR.[23] Targeting flanking sequences TS1 (572 bp) and TS2 (527 bp) were amplified using primer pair P1 and P2 and primer pair P3 and P4. TS1, TS2, and FRT-*hph*-FRT were joined by splicing overlap extension PCR (SOE-PCR) to produce a 2702 bp amplicon (Figure S1 of the Supporting Information). Arabinose-induced electrocompetent *K. pneumoniae* MGH 78578/pKOBEGApra maintained at 30 °C was electroporated with 100 ng of the SOE-PCR product, and transformants were recovered on LB/200 μg/mL hygromycin agar at 37 °C after overnight culture. Several hygromycin resistant colonies were examined, and the Δ*cld* mutant was validated by PCR analysis (Figure S1 of the Supporting Information). Bacteria and plasmids used for *cld* mutagenesis are listed in Table S1 of the Supporting Information.

Phenotypic Characterization of the Δ*cld* Strain. Frozen (−80 °C) glycerol stocks of wild-type (WT) and Δ*cld* strains of *K. pneumoniae* were revived by streaking on Luria broth (LB) agar and LB agar/hygromycin B (75 mg/mL) plates, respectively. Hygromycin B was used in all growth experiments to maintain the mutant free of contamination. Single colonies were inoculated into 5 mL of LB or LB with hygromycin B and grown to an OD_{600} of 0.4. Cells were harvested in microcentrifuge tubes and washed three times with M9 medium [0.2% (v/v) glycerol, 58 mM K_2HPO_4, 22 mM Na_2HPO_4, 85 mM NaCl, and 18.7 mM NH_4Cl] supplemented with the following trace elements in 134 μM EDTA: 6.15 μM ZnO, 570 nM $CuCl_2{\cdot}2H_2O$, 340 nM $CoNO_3{\cdot}6H_2O$, and 1.6 μM H_3BO_3. Cells were resuspended to a final optical density at 600 nm (OD_{600}) of 0.4 and used as a uniform inoculate (1:100) for all experiments.

For determination of minimal inhibitory concentrations of ClO_X^- (X = 2−4), cells were inoculated into 10 mL of anaerobic, N_2-purged medium in sealed glass crimp-topped bottles containing increasing concentrations of $NaClO_2$, $NaClO_3$, or $KClO_4$ (0.5−200 mM) and 50 mM KNO_3. The sealed bottles were placed in a 37 °C incubator with gentle shaking. The minimal inhibitory concentration (MIC) was defined as the lowest concentration of a reagent that would inhibit the visible growth of *K. pneumoniae* after incubation for 24 h.[24] No-nitrate controls were conducted in tandem under aerobic conditions. Finally, for generation of growth curves, cells were inoculated into aerobic media and their growth was monitored via periodic measurement of their OD_{600} over time.

Growth, Purification, and Characterization of Wild-Type (WT) and Mutant *Kp*Cld. DNA containing the full-length coding region of chlorite dismutase from *K. pneumoniae* MGH 78578 (GenBank accession number CP000650.1) was amplified via PCR with primers KpCldFor (5′-CGC CATATG AAT ACA CGA TTA TTT ACG TTC GCT GG-3′) and KpCldRev (5′-TTT GGATCC CTA GGC CGG CTC ATG CA-3′) from a *K. pneumoniae* genomic DNA template (added cut sites for NdeI and BamHI at the 5′ and 3′ ends underlined, respectively). The product was subsequently cloned into the pET-15b (Merck/Novagen) expression vector for production of protein with an N-terminal His tag. The Y62F and W97F mutants of *Kp*Cld and the Y118F mutant of *Da*Cld were generated from the WT via PCR-based single-codon substitution using a QuikChange kit. The W227F, W155F, and W156F mutants of *Da*Cld were generated in a similar manner and were available from prior work.[25]

All *Kp*Clds were expressed in *Escherichia coli* Tuner (DE3) cells (Merck/Novagen) grown in Terrific Broth (TB) with ampicillin (100 μg/mL). Expression cultures were grown at 37 °C in a shaker incubator (250 rpm) to midlogarithmic phase (OD_{600} = 0.5). Isopropyl β-D-thiogalactopyranoside (IPTG, 1 mM) and δ-aminolevulinic acid (50 mg/L) were added to induce heme protein expression, and the temperature was lowered to 20 °C. After 16 h, cell pellets were collected by centrifugation and stored at −80 °C. Cells were thawed and resuspended [20 mM phosphate buffer, 500 mM NaCl, 20 mM imidazole, and 1 mM phenylmethanesulfonyl fluoride (pH 7.4)] and lysed by pulsed sonication on ice (7 min). The lysates were clarified by centrifugation and supernatants loaded onto a

dx.doi.org/10.1021/bi501184c | *Biochemistry* 2015, 54, 434−446

20 mL HisTrap column. The protein was eluted using a 20 to 500 mM linear gradient of imidazole in resuspension buffer. Eluted proteins were screened by sodium dodecyl sulfate−polyacrylamide gel electrophoresis and pure fractions buffer-exchanged into 0.1 M phosphate buffer (0.1 M, pH 6.8) using Amicon centrifuge concentrators (molecular weight cutoff of 10000). Pure protein was concentrated to 10 mg/mL (20% glycerol), frozen in liquid N_2, and stored at −80 °C. All *Kp*Cld concentrations are given as heme-bound monomer, where [heme] and [protein] were determined by the pyridine hemochrome and Bradford assays,[26] respectively.

Measurement of Initial Rates of Chlorite-Decomposing Activity in the Steady State. A luminescence-based probe was used to measure O_2 evolution by *Kp*Cld during chlorite decomposition under steady state conditions. Samples included 12 nM WT *Kp*Cld and 0.05−2 mM chlorite in the following buffer solutions: 50 mM phosphate-citrate (pH <6), 100 mM phosphate (pH 6−8), or 100 mM glycine (pH >8). The probe was equilibrated in the buffer/chlorite solution for 5−10 min prior to initiation of the reaction by introduction of enzyme. Kinetic traces were recorded at 1 s intervals for 3−10 min.

Monitoring Heme Chromophore Loss Caused by $NaClO_2$ or NaOCl. Samples (10 μM, 200 μL) of heme-containing *Kp*Cld were titrated in UV−visible cuvettes with a concentrated chlorite or hypochlorite stock (600 mM) added in 1 μL increments [all solutions in 0.1 M citrate-phosphate buffer (pH 6.6)]. Samples were allowed to come to equilibrium following each addition and corrected for dilution.

Chromophore loss was also monitored over time following the addition of varying amounts of NaOCl as a function of pH. Reactions were conducted in 0.1 M citrate-phosphate at pH 6−8. Samples (10 μM, 200 μL) of heme-containing *Kp*Cld in UV−visible cuvettes were manually mixed with a NaOCl stock, yielding final NaOCl concentrations of 0−1 mM (0−2000 equiv). Spectra were measured every 6 s after mixing. The absorbance at the Soret band maximum (409 nm) was plotted versus time and fit to a single-exponential equation to obtain a first-order rate constant (k_{obs}). Values of k_{obs} measured at a given pH were plotted versus NaOCl concentration to obtain second-order rate constants (k is the slope).

Measurement of Residual Activities and Turnover Numbers. Chlorite's potency as a suicide substrate was assessed by the method of Silverman.[27] Briefly, 5 μM samples of *Kp*Cld were incubated for 1 h at room temperature with an increasing number of equivalents of chlorite up to 3×10^4, with or without 0.5 mM added guaiacol, MCD, or ABTS [0.1 M citrate-phosphate buffer (pH 6.6)]. Reaction mixtures were dialyzed against chlorite-free buffer for two 1 h cycles to remove any unreacted substrate. The remaining *Kp*Cld reactivity was measured using a Clark oxygen electrode by adding 5 μL of each dialysate to 1.5 mL of 2 mM chlorite and measuring the initial rate of O_2 production. Rates were measured three times, corrected for dilution, and averaged. Residual activity was computed by referencing the activity remaining after incubation in a given chlorite concentration to the activity of the zero chlorite control. The turnover number, defined as the total number of molecules of chlorite catalyzed per *Kp*Cld heme before the catalyst is irreversibly inactivated, was obtained by extrapolating a plot of residual activity versus $[ClO_2^-]/[KpCld]$ to the x-intercept.

Vibrational Characterization of *Kp*Cld. Resonance Raman (rR) spectra were obtained with 413.1 or 441.6 nm excitation from a Kr^+ or HeCd laser, respectively, using the 135° backscattering geometry for collection of Raman-scattered light. The spectrometer was calibrated against Raman frequencies of toluene, dimethylformamide, acetone, and methylene bromide. Spectra were recorded at ambient temperature from samples in spinning 5 mm NMR tubes. UV−visible absorbance spectra were recorded from the rR samples before and after spectral acquisition to assess whether sample integrity had been compromised by exposure to the laser beam. The laser power at ferric and ferrous samples ranged from 5 to 10 mW; no spectral artifacts due to photoinduced chemistry were observed with these irradiation powers. Ferric *Kp*Cld samples for the rR pH dependence study were prepared in the following 100 mM buffers: potassium phosphate (pH 5.7−7.5), Tris-HCl (pH 8.6−9.7), and borate buffer (pH 10.1).

Electron Paramagnetic Resonance (EPR) Spectroscopy. The 9 GHz EPR spectra were recorded on a Bruker EleXsys E500 spectrometer equipped with a standard Bruker ER 4102 X-band resonator and a liquid helium cryostat (Oxford Instruments, ESR 900). The spectra for WT *Kp*Cld at pH 6.0 were recorded at 4 K, a microwave power of 1 mW, a modulation amplitude of 4 G, and a modulation frequency of 100 kHz. The spectra at pH 8.0 were recorded at 12 K, a modulation amplitude of 10 G, a microwave power of 0.5 mW, and a modulation frequency of 100 kHz. Spectra for the mutant *Kp*Clds were recorded at 4 K, a microwave power of 1 mW, a modulation amplitude of 4 G, and a modulation frequency of 100 kHz. To avoid significant changes in pH upon freezing, Tris-maleate buffer, which covers the pH range from 5.2 to 8.6 with minor changes (0.1 pH unit) upon freezing, was used. No effect on the ferric EPR signal was observed for the Tris-maleate buffer as compared to that with phosphate buffer when using the same pHs. Typically, EPR samples of ferric *Kp*Cld and *Da*Cld [in 0.1 mM Tris-maleate (pH 6.0 or 8.0) and at 0.6 mM enzyme] were measured in 4 mm quartz tubes. The buffer exchange in the pH range of 5.0−8.0, conducted with Centricon microconcentrators (Amicon), could be reversibly obtained without enzyme precipitation, degradation, or iron release as judged by the electronic absorption and EPR spectra recorded after each buffer exchange. Freezing and thawing cycles at high enzyme concentrations used for the EPR characterization did not induce any enzyme precipitation or changes in the heme environment.

RESULTS

Heme Environment in *Kp*Cld As Measured by UV−Vis and rR. *Kp*Cld has a reversible pH-dependent transition in UV−visible spectrophotometric titrations. Experiments in which the enzyme was titrated with base (Figure 3A) and acid (data not shown) yielded the same pK_a. Fits of UV−vis data at 390 nm (Figure 3A, inset), 413 nm, and 574 nm (not shown) indicated a pK_a of 8.3, the same as that reported for the *Azospira oryzae* Cld[28] and slightly lower than that for Clds from *Ideonella dechloratans* (8.5)[29] and *D. aromatica* (8.7).[5] Heme proteins with neutral proximal histidine ligands have pK_a values [heme oxygenase-1 and -2 (7.6 and 8.5, respectively), *Sm*FixL (9.6), and HmuO (9.0)] lower than the pK_a values of those with a proximal histidinate [peroxidases (pK_a values of 11−12)].[30−32] Consistent with a pK_a in this range, the Fe(II)−His vibrational frequency measured by rR for *Kp*Cld suggests a charge-neutral proximal histidine (Figure S2 of the Supporting Information; discussed further below).

dx.doi.org/10.1021/bi501184c | *Biochemistry* 2015, 54, 434−446

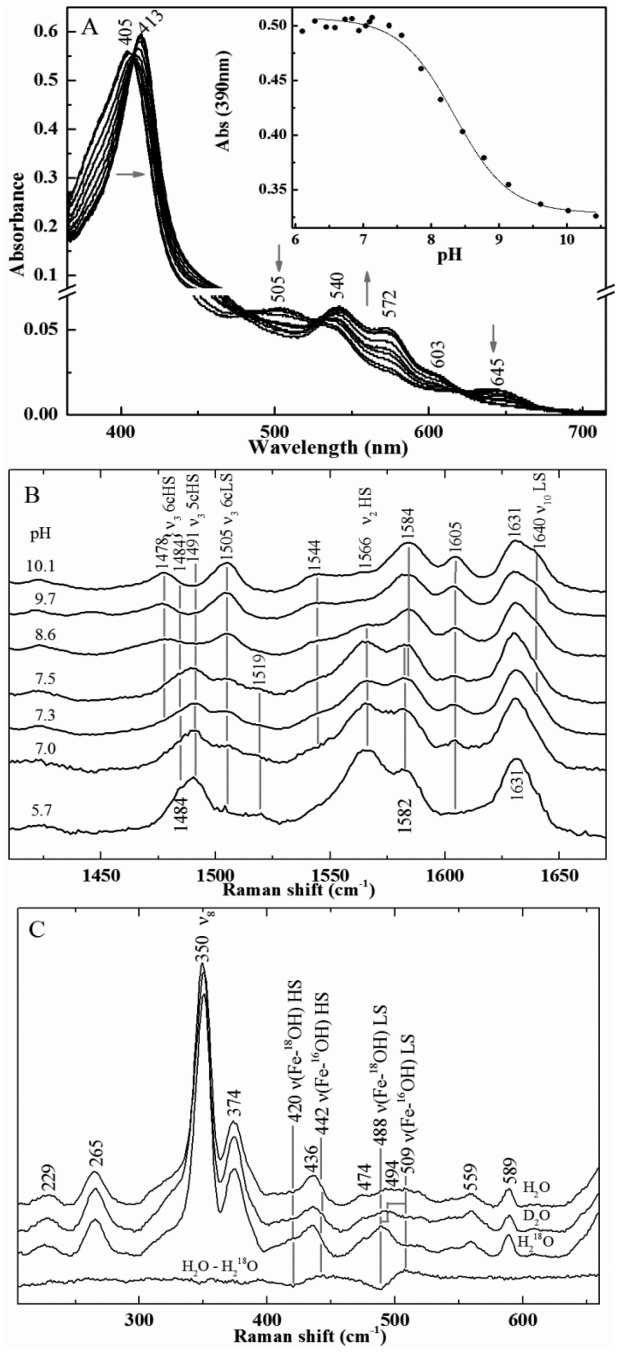

Figure 3. pH-dependent behavior of *Kp*Cld indicates a water-accessible heme. (A) UV−visible pH titration of *Kp*Cld. Spectra shown at pH 7.13, 7.38, 7.85, 8.1.4, 8.46, 8.78, 9.14, 9.61, 10.07, and 10.43. Arrows indicate the direction of the absorbance change with pH. The inset shows the absorbance at 390 nm as a function of pH; a least-squares fit to the data (●) gives a pK_a of 8.3. (B) Speciation of ferric *Kp*Cld as observed in rR pH titration. Resonance Raman spectra were obtained with 413.1 nm excitation at the indicated pH values. (C) Soret-excited rR spectra of the oxygen isotopologs of alkaline *Kp*Cld [50 mM Ches (pH 9.8)]. The top three spectra were measured in the indicated solvent at identical acquisition times. The bottom trace is the difference spectrum generated by a 1:1 digital subtraction (H_2O − $H_2{}^{18}O$).

At pH 6.0, ferric *Kp*Cld exhibits a Soret band maximum at 405 nm, a broad α/β band envelope at 505 nm with a small shoulder at 540 nm, and a charge transfer (CT) band at 645 nm (Figure 3A). This spectrum is similar to that reported for the related dimeric *Nw*Cld (405, 506, 543, and 640 nm) and the pentameric Cld from *Candidatus Nitrospira defluvii* at pH 7.0,[10,11] but different from Clds from *D. aromatica* (393, 506, and 648 nm, pH 7.0), *A. oryzae* (392−394 nm), and *I. dechloratans* (392, 509, and 648 nm, pH 7).[5,9,29] The latter three proteins, which come from perchlorate respirers, share similar five-coordinate, high-spin (5cHS) heme sites, pentameric oligomerization states, and hydrophobic, solvent-enclosed heme environments, to which their blue-shifted Soret bands have been attributed. In contrast, the visible spectrum of acidic *Kp*Cld corresponds to a mixture of coordination states; this is confirmed by its rR spectra (below).

The rR spectra (Figure 3B) of ferric *Kp*Cld in a mildly acidic solution have a broad HS ν_3 envelope spanning 1482−1490 cm^{-1}, consistent with a mixture of six-coordinate, high-spin (6cHS) and 5cHS heme. The temperature dependence of the HS ν_3 envelope supports the presence of 5cHS and 6cHS hemes. When the temperature of ferric *Kp*Cld is decreased from 19 °C at pH 6.0, the 6cHS intensity of the ν_3 envelope at 1484 cm^{-1} increases at the expense of the 5cHS component at 1491 cm^{-1}. Below −14 °C, the envelope narrows to a single band centered at 1484 cm^{-1}, indicating complete conversion of the HS heme to a 6c complex that is likely an aqua complex, whose formation is exothermic (Figure S3 of the Supporting Information). The acid−base behavior of this complex (see below) supports this assignment. These data indicate that a considerable fraction of the resting HS enzyme is coordinatively saturated at near-physiological temperatures. In contrast, the acidic form of *Da*Cld contains only 5cHS heme.[5]

Another small ν_3 band occurs at 1505 cm^{-1} at 19 °C and pH ∼6 (Figure 3B). The intensity of this band increases in concert with that of a new 6cHS band at 1478 cm^{-1} as the pH is increased. Bands in the 1505 cm^{-1} frequency range can be consistent with 6cLS species or 5cQS (5c quantum mechanical spin admixture of $S = {}^3/_2$ and $S = {}^5/_2$ ferric heme). The appearance of UV−visible bands near 572 nm (typical for 6cLS species) and 646 nm (CT) at pH 7.0 argue for assignment of the ν_3 band to a 6cLS species. At pH 10, ferric *Kp*Cld has a Soret maximum at 413 nm, α/β bands at 572 and 540 nm, and small absorbance bands near 490 and 603 nm. The 572 and 540 nm bands are consistent with a 6cLS complex, while the bands at 490 and 603 nm are suggestive of a 6cHS species (Figure 3A). These features are very similar to those reported for alkaline ferric *Da*Cld.[5] The mixture of spin states suggested by the UV−visible spectrum is confirmed by the appearance of two ν_3 bands at 1478 and 1505 cm^{-1} in the rR spectrum of alkaline *Kp*Cld. Growth of these bands is accompanied by the appearance of a shoulder at 1640 cm^{-1}, which can be attributed to ν_{10} for 6cLS heme, and a 2 cm^{-1} upshift in the frequency of ν_4 (not shown), both indicating growth in the population of 6cLS heme. The formation of heme hydroxides is often characterized by parallel growth in the intensity of bands arising from 6cHS and 6cLS hemes, which indicate its presence as a thermal spin state equilibrium. Similar mixtures attributed to such equilibria have been reported for a number of heme proteins, including the alkaline forms of *Da*Cld, myoglobin, hemoglobin, *Mycobacterium tuberculosis* HbN, and *Sm*FixL.[5,33−36]

To determine whether the sixth ligand in *Kp*Cld is hydroxide at pH 9.8, the ν_{Fe-OH} modes were identified by isotopic substitution (Figure 3C). Bands at 509 and 442 cm^{-1} were assigned to the Fe−OH stretching modes for the LS and HS

dx.doi.org/10.1021/bi501184c | *Biochemistry* 2015, 54, 434−446

heme hydroxides, respectively. The LS ν_{Fe-OH} band shifts to 494 cm^{-1} in D_2O and to 488 cm^{-1} in $H_2{}^{18}O$. In the case of the HS heme, no deuterium shift is detected. In $H_2{}^{18}O$, the $\nu_{Fe-{}^{18}OH}$ band shifts by 22 cm^{-1} to 420 cm^{-1}. Thus, the pK_a of 8.3 corresponds to the formation of the *Kp*Cld−OH complex. Consistent with our previous report about the *Da*Cld−OH complex,[5] the ν_{Fe-OH} bands of both HS and LS *Kp*Cld−OH complexes fall at the low end of the Fe−OH stretching frequency range for heme hydroxides.

Finally, the UV−visible spectrum of ferrous *Kp*Cld (pH 7.0) generated by reduction of the ferric protein with a 12-fold redox excess of sodium dithionite exhibited a Soret band maximum at 433 nm, typical of 5cHS ferrous heme, and α/β bands at 586 and 555 nm, respectively (Figure S2 of the Supporting Information). The 413.1 nm excited Fe(II) *Kp*Cld spectrum at pH 7.0 has a ν_4 at 1356 cm^{-1}, typical of ferrous heme, and a ν_3 at 1472 cm^{-1}, typical of 5cHS ferrous heme. The 441.6 nm excited Fe(II) *Kp*Cld spectrum revealed an Fe−His stretching band at 229 cm^{-1}, 7 cm^{-1} higher than that observed for *Da*Cld (222 cm^{-1} at pH 6.8),[5] consistent with the Fe−His bond being slightly stronger in *Kp*Cld assuming similar normal mode compositions in the two enzymes.

Structural Features of the *Kp*Cld Heme Environment, Including Second-Sphere Interactions As Revealed by 9 GHz EPR Spectroscopy. EPR spectroscopy is a sensitive probe of the extended hydrogen bonding network of heme active sites, including structural water molecules as well as second-sphere (and beyond) amino acid residues.[37,38] In the absence of a crystal structure for *Kp*Cld and to expand the structural view of the heme site provided by rR, the ferric EPR spectra of wild-type *Kp*Cld and key variants in its heme extended environment were examined as a function of pH. These were compared to their *Da*Cld counterparts, for which the WT crystal structure has been determined.[8]

Figure 4 shows the 9 GHz EPR spectra of wild-type *Kp*Cld recorded at cryogenic temperatures (4 and 12 K). The ferric EPR spectrum of *Kp*Cld remained invariant in the pH range of 5.5−7.9 (top, black trace) but showed a dramatic change at pH 8.0 (top, gray trace). At pH 6.0 (Figure 4, top, black trace), the EPR spectrum of *Kp*Cld showed an axial signal, with observed effective g values of $g_\perp$ = 5.92 and $g_\parallel$ = 1.99, consistent with a ferric high-spin species. At pH 8.0 (Figure 4, top, gray trace), the *Kp*Cld EPR spectrum showed a distinct LS ferric species, with effective g values of g_{Cx} = 2.54, g_{Cy} = 2.19, and g_{Cz} = 1.87. The almost complete conversion of the ferric EPR signal from high-spin to low-spin at pH 8.0, observed in frozen solutions, differs from the more gradual effect observed in the rR experiments in solution (Figure 3B) and most possibly reflects the preferential configurations of the heme environment locked in the frozen samples. The ferric LS EPR spectrum overall is consistent with a nitrogenous amino acid side chain not directly coordinated to the heme iron, in the vicinity of the Fe−OH bond revealed by the rR characterization described in the previous section. The relatively smaller contribution of another LS signal with a large g_{max} of 3.10 (the other two components being very weak and too broad to be detected) consistent, in this case, with a nitrogenous ligand on the heme distal side[8] was also observed. The identity of this ligand is not known. It is possible that, even after thorough dialysis, some imidazole used in the purification of the protein remained in the active site. Alternatively, repositioning of the distal arginine, with a deprotonated guanidinium group replacing water molecules close to the iron [for example, in the structural water molecules

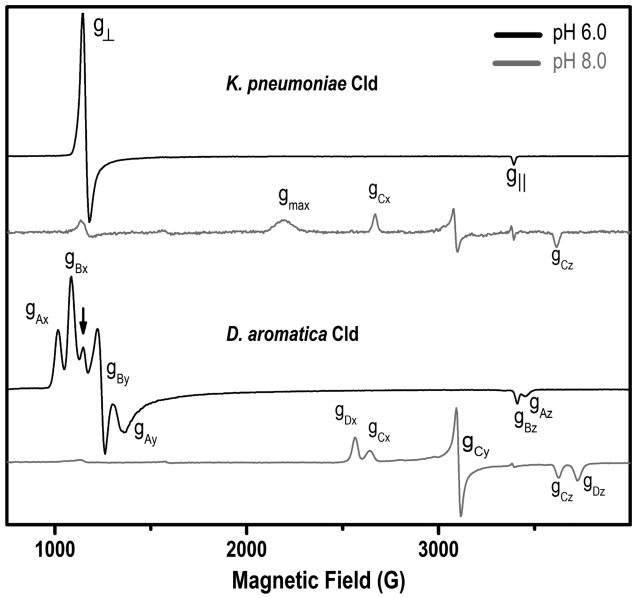

Figure 4. 9 GHz EPR spectra of ferric Clds from *K. pneumonia* (top) and *D. aromatica* (bottom) as a function of pH. A spin switch from high-spin ferric (black trace) to low-spin ferric (gray trace) is observed at pH ≥8.0. The conversion of the high-spin ferric signal was estimated to be 95% in *Da*Cld and 85% in *Kp*Cld. The spectra at pH 6.0 were recorded at 4 K, a microwave power of 1 mW, a modulation amplitude of 4 G, and a modulation frequency of 100 kHz. The spectra at pH 8.0 were recorded at 12 K, a modulation amplitude of 10 G, a microwave power of 0.5 mW, and a modulation frequency of 100 kHz.

shown in the *Nw*Cld structure (Figure 2)], could be envisioned if considering the crystal structures of the *N. defluvii* Cld with thiocyanate bound in the sixth coordination position of the heme.[10]

The EPR spectra of *Da*Cld differed substantially from those of *Kp*Cld. Specifically, the spectrum at pH 6.0 showed the contribution of two ferric HS EPR signals (Figure 4, labeled with subscripts A and B), with effective g values of (g_{Ax} = 6.67, g_{Ay} = 5.20, g_{Az} = 1.96) and (g_{Bx} = 6.25, g_{By} = 5.24, g_{Bz} = 1.99). Two distinct LS ferric species (Figure 4, subscripts C and D), with effective g values of (g_{Cx} = 2.56, $g_{Cy} \approx$ 2.18, g_{Cz} = 1.87) and (g_{Dx} = 2.64, $g_{By} \approx$ 2.18, g_{Bz} = 1.82), were consistently observed at pH 8.0. These observations of two HS and two LS EPR signals are consistent with our earlier reports that closed (more active) and open (less active) *Da*Cld conformers are present between pH 5.6 and 9.1.[16]

To improve our understanding of the lack of pH-induced changes in the HS EPR spectra as well as the difference in ferric heme signals of the various Clds, structurally conservative mutations at highly conserved Trp and Tyr residues within hydrogen bonding distance of the heme propionates were constructed. Specifically, the crystal structures of the *Da* and *Nw* Clds show that a highly conserved tyrosine (Tyr118, Figure 2D; Tyr62 in *Kp*Cld) appears to make hydrogen bonding contacts to both heme propionates via its phenol oxygen and amide nitrogen. The indole N atom of a conserved tryptophan (Trp155 of *Da*Cld or Trp97 of *Kp*Cld) lies within hydrogen bonding distance of one heme propionate. A second strictly conserved Trp (Trp156 of *Da*Cld or Trp98 of *Kp*Cld) is sterically close to the same propionate but oriented such that the indole nitrogen cannot form a hydrogen bond to it. Accordingly, we anticipated that substitutions of these conserved residues could considerably affect the orientation

dx.doi.org/10.1021/bi501184c | *Biochemistry* 2015, 54, 434−446

of the propionate(s) and/or heme planarity, resulting in measurable changes in the ferric EPR spectra.

Figure 5 shows dramatic changes observed in the ferric EPR spectra of *Kp*Cld and *Da*Cld upon mutation of these active site

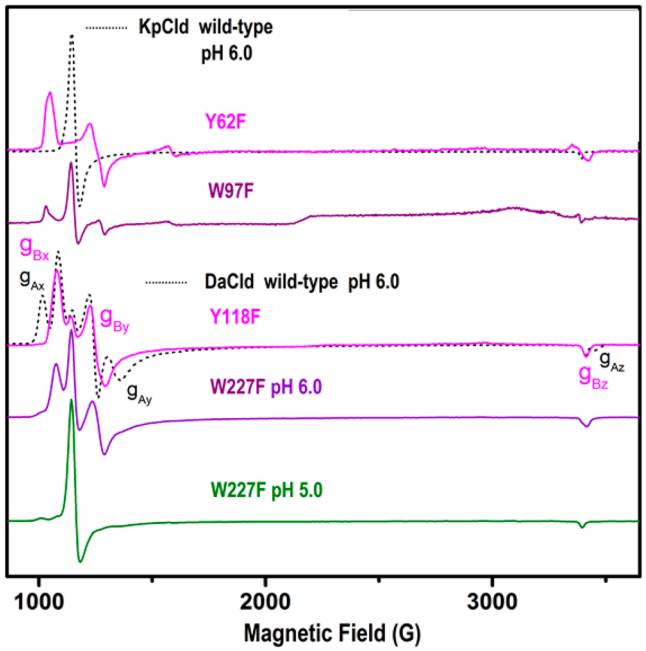

Figure 5. 9 GHz EPR spectra of selected mutations on the heme environment of *Kp*Cld (top) and *Da*Cld (bottom) at pH 6.0. Both spectra of the wild-type Clds (black dotted traces) are shown for comparison. Figure 2D shows the crystallographic structure of the extended heme environment of *Nw*Cld (PDB entry 3QPI), in which the amino acid residues at positions equivalent to those mutated in *Kp*Cld (Y62F and W97F, at the same positions as Tyr118 and Trp155) are shown. The other Trp mutated in *Da*Cld (Trp227) is not conserved in *Nw*Cld or *Kp*Cld. Spectra were recorded at 4 K, a microwave power of 1 mW, a modulation amplitude of 4 G, and a modulation frequency of 100 kHz.

residues. The axial HS EPR signal of WT *Kp*Cld (Figure 5, top, dotted black trace) fully converted to a rhombically distorted spectrum in the Y62F mutant (Figure 5, top, magenta trace), with the contribution of two species [effective g values of (6.46, 5.39, 1.98) and (6.57, 5.54, 1.99)]. The W97F mutation in *Kp*Cld induced a partial conversion of the wild-type axial signal to one of the rhombically distorted HS forms of the Y62F variant, with effective g values of (6.57, 5.54, 1.99), with a contribution of the 6cLS form with a large g_{max} of 3.10 (Figure 5, top, purple trace). The same LS high-g_{max} form was observed in WT *Kp*Cld, but only at basic pH (Figure 4, top, gray trace). In the Y118F mutant of *Da*Cld, positionally equivalent to Y62F in *Kp*Cld, the EPR component with the largest rhombic distortion disappears (Figure 5, bottom, magenta trace). The ferric EPR spectrum of the Y118F *Da*Cld variant then becomes very similar to the previously reported rhombic EPR spectra of the Clds from *A. oryzae* and *I. dechloratans*,[9,29] and also similar to that of Y62F *Kp*Cld. Accordingly, these results show that breaking the hydrogen bonds to the propionates allows more flexibility of the heme.

To explore these differences further, we investigated the *Da*Cld W227F mutant. This residue is conserved among the Clds from known perchlorate respirers but not in the dimeric Clds (Figures 1 and 2) and could represent a key differentiation between the two groups. Trp227 is not connected to the heme by hydrogen bonds yet is sterically close to those other residues having hydrogen bonding interactions to the heme. Interestingly, two significant changes were observed in the ferric EPR spectrum of W227F *Da*Cld relative to WT: the disappearance of the component with the largest rhombic distortion, as in *Da*Cld Y118F, and an increase in the contribution of the axial EPR signal (Figure 5, bottom, violet trace). Moreover, the ratio of the axial and rhombically distorted signals of the W227F *Da*Cld EPR spectrum became pH-dependent, as in the case of *Burkholderia pseudomallei* KatG,[39] fully converting to the axial signal at pH 5.0 (Figure 5, bottom, green trace). Hence, the resulting EPR spectrum for *Da*Cld W227F at pH 5.0 is the same as that of wild-type *Kp*Cld (Figure 5, top, dotted black trace). Notably, the mutant protein could be isolated in a stably heme-bound state at low pH if concentrated and frozen immediately following purification (see Experimental Procedures).[25] These results reinforce the idea that second-sphere coordination influences the electronic structure of the heme iron. They also suggest that the conserved residue Trp227 is indeed important for distinguishing the heme environments of *Da*Cld and *Kp*Cld even though it is not directly connected to the heme via hydrogen bonding.

***Kp*Cld Exhibits Chlorite-Decomposing Activity.** *Kp*Cld is a competent catalyst of chlorite decomposition; values of k_{cat} and k_{cat}/K_M are maximal near pH 5.0, at $(1.9 \pm 0.2) \times 10^3$ s^{-1} and $(2.5 \pm 0.4) \times 10^6$ M^{-1} s^{-1}, respectively (20 °C) (Figure S4 of the Supporting Information). These values are approximately 10-fold lower than the corresponding parameters for *Da*Cld measured at its pH 5.2 optimum (4 °C): $k_{cat} = (2.0 \pm 0.6) \times 10^4$ s^{-1}, and $k_{cat}/K_M = (3.2 \pm 0.4) \times 10^7$ M^{-1} s^{-1}.[5] A pH optimum between 5 and 6 was recently measured for the k_{cat} for the *N. defluvii* Cld.[10,40]

Steady state pH−rate profiles for *Kp*Cld (Figure S4 of the Supporting Information) and *Da*Cld[5] are broadly similar, with each protein possessing a more active acidic form and less active alkaline form. Turning points in the plots of log k_{cat} versus pH were fit at pH 6.5 and 8.7 (*Da*Cld).[5] A transition from a highly active low-pH form to a less active alkaline form is apparent near pH 7 for *Kp*Cld. Turning points in log−log plots of kinetic constants are associated with pK_a values. Though not explicitly assigned here for *Kp*Cld, the lower-pH turning point in *Da*Cld was previously assigned to the distal arginine, first modeled as an explicit deprotonation and later associated with movement of the distal pocket Arg between less reactive "out" (alkaline) and more reactive "in" (acidic) conformations (Figure 2). The latter model is supported by both spectroscopic evidence and reactivity data with H_2O_2.[5,6,16]

Chlorite Acts as a Potent Suicide Substrate. Titration of *Kp*Cld with chlorite (Figure 6A) demonstrated near-complete elimination of the heme's Soret band following exposure to roughly $(6.0 \pm 0.3) \times 10^3$ equiv of the oxidant. This value is intermediate between *Da*Cld's (2.0×10^4) and *Sa*Cld's ($\leq$5).[5,14] To relate heme destruction quantitatively to the loss of catalytic activity, *Kp*Cld's turnover number was measured (Figure 6B). A line fit to a plot of residual activity versus chlorite equivalents intercepts the x-axis at 5.3×10^3. The same data could also be fit to an exponential decay curve, consistent with some protection of the enzyme from degradation by the accumulation of high product concentrations.[41] The exponential curve predicts heme degradation after exposure to even fewer equivalents of chlorite, that is, the number of equivalents extrapolated from where the initial,

dx.doi.org/10.1021/bi501184c | *Biochemistry* 2015, 54, 434−446

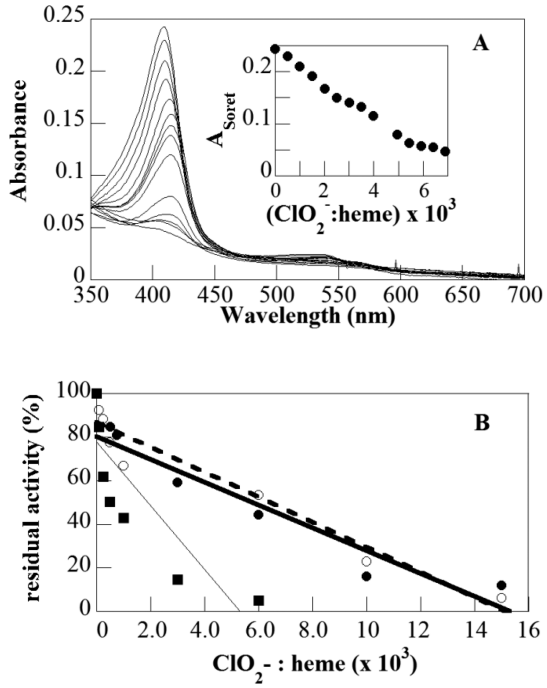

Figure 6. Chlorite acts as a suicide substrate and is rescued by H atom donors and chlorination substrates. (A) ClO_2^- was added in 300 equiv increments and the heme chromophore observed to diminish to baseline after roughly 6×10^3 equiv. The inset shows the Soret band absorbance plotted vs added chlorite equivalents. (B) Residual enzymatic activity following incubation with increasing equivalents of chlorite. Linear extrapolation to the *x*-axis yields the turnover number: no additives (■, 5.3×10^3), with added ABTS (●, —, 1.5×10^4), and with added MCD (○, – – –, 1.5×10^4).

linear phase intercepts the *x*-axis. The number extrapolated from a straight line fit to all of the data is therefore likely an upper limit for turnovers.

The measured turnover number is similar to but slightly less than the number of equivalents required to completely eliminate the Soret band (Figure 6A, inset), suggesting that loss of activity is correlated with destruction of the heme and also some degree of protein damage. Consistent with these results, a detailed study of chlorite-mediated damage to the pentameric Cld from *N. defluvii* showed that chlorite effected damage in a number of ways, including oxidation of methionine residues, chlorination of aromatic side chains, and heme lysis.[42]

H Atom Donors and Chlorination Traps Increase *Kp*Cld's Turnover Number. The turnover number was remeasured in the presence of excess guaiacol and ABTS, which can act as sacrificial hydrogen atom donors toward highly reactive oxidants. These could include ferryl heme species, (H)OCl produced as intermediates in the O_2-generating reaction, or chlorine dioxide (ClO_2) from the one-electron oxidation of chlorite by a ferryl heme. In the presence of guaiacol, the turnover number for *Da*Cld increased by approximately 10-fold.[3] Here, in guaiacol or ABTS, the turnover number increased more modestly, to 1.5×10^4 (~2-fold larger). The same trend was observed in the presence of MCD, a trap used to detect chlorinating agents (HOCl, ClO_2, or OCl^-) in enzymatic reactions.[43,44] These results indicated that a species capable of reacting with guaiacol, ABTS, and MCD was responsible for chlorite-mediated inactivation of *Kp*Cld.

(H)OCl Is Produced by *Kp*Cld during Steady State Turnover with Chlorite. To directly detect the species generated during turnover, the reaction between ClO_2^- (3 mM) and *Kp*Cld (0.1 μM) was monitored via UV–vis under steady state conditions. Unreacted chlorite was quantified by iodometric titration. ClO_2^- decomposition was incomplete: 36 ± 5% of the initially present chlorite had degraded by the end of the experiment, indicating $(6.7 \pm 0.3) \times 10^3$ turnovers per heme; representative results are shown, and turnover numbers are an average of three experiments (Figure 7A). Chlorite decomposition moreover occurred with no observable accumulation of ClO_2 (ε_{262} = 160 M^{-1} cm^{-1}). When 50 μM MCD was added to the same reaction mixture, conversion of the MCD to DCD could be readily detected via the loss of the MCD chromophore (Figure 7B). The reaction with ClO_2^- also

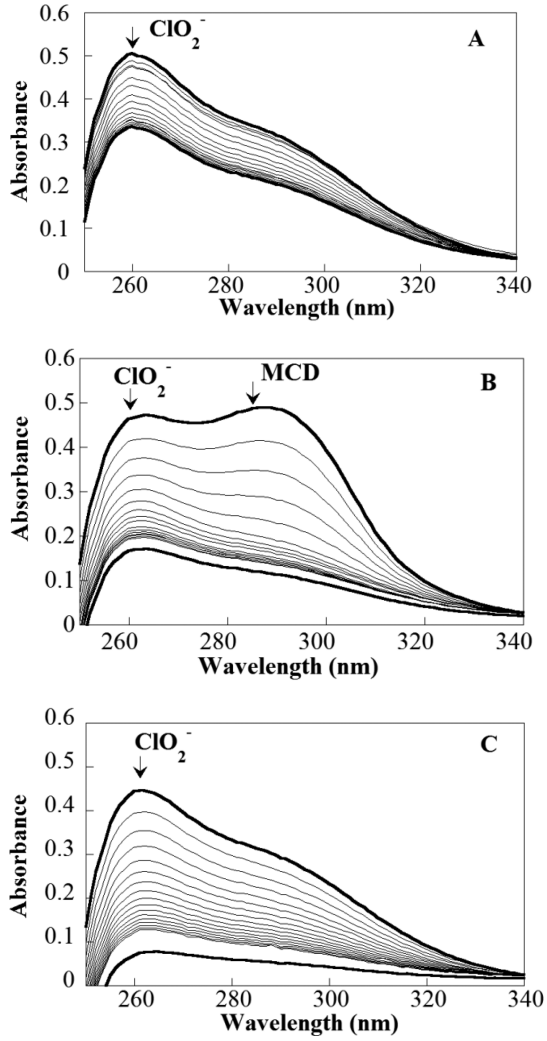

Figure 7. Chlorite decomposition is enhanced by the presence of (H)OCl trapping agents. (A) An inhibitory concentration of ClO_2^- (3 mM) was added to a catalytic amount (0.1 μM) of *Kp*Cld [0.1 M citrate-phosphate (pH 6.6)]. Spectra were measured every 30 s (gray lines) until the reaction had reached completion (black lines; t = 0 and 30 min); 36% of the initially present ClO_2^- decomposed without the appearance of ClO_2. (B) In the presence of 50 μM MCD and the same amount of ClO_2^-, the turnover number more than doubles. MCD's chromophore disappears, consistent with conversion to the chlorinated product DCD. (C) Colorless DMSO, used as a HOCl-specific trap, enhances ClO_2^- turnover to a similar extent.

dx.doi.org/10.1021/bi501184c | *Biochemistry* 2015, 54, 434–446

proceeded much closer to completion: 73 ± 5% consumed, or (1.4 ± 0.1) × 10^4 turnovers per heme.

To distinguish definitively between HOCl or ClO_2 as the MCD-reactive species, DMSO was assayed for its ability to enhance turnover. DMSO has previously been used as a highly selective trapping agent for HOCl in aqueous ClO_2/ClO_2^- mixtures.[45] Neutral HOCl is the reactive species (HOCl ⇆ OCl^- + H^+; pK_a = 7.5), serving as an electrophilic oxidant via transfer of OH^+ to a nucleophilic acceptor substrate (here, the lone pair of electrons on the sulfoxide).[45] When the *Kp*Cld/chlorite reaction shown in Figure 7A was monitored in the presence of 50 μM DMSO (Figure 7C), the reaction proceeded rapidly and nearly to completion [86 ± 7%; (1.6 ± 0.2) × 10^4 turnovers per heme]. This strongly suggested that HOCl and not ClO_2 is released from *Kp*Cld during turnover with ClO_2^-. The results in panels A and B of Figure 6 are moreover consistent with the measured turnover number for chlorite and expected increases in turnover afforded by MCD (Figure 6), and they support the conclusion that MCD's protective function is due to its reaction with HOCl.

Hypochlorous Acid Avidly Degrades *Kp*Cld's Heme. To quantify the influence of chlorite-derived HOCl on heme degradation, the effect of exogenously added sodium hypochlorite on the heme spectrum was measured titrimetrically at pH 6.6, where it is expected to equilibrate rapidly to form HOCl. The spectrum diminished to baseline following addition of 800 ± 20 equiv of NaOCl (Figure S5 of the Supporting Information), versus (6.0 ± 3) × 10^3 equiv of ClO_2^- (Figure 3A). If HOCl alone were responsible for catalytic inactivation, this would suggest that approximately one in eight turnovers would lead to HOCl rather than O_2 during catalysis of ClO_2^-. This number is likely an upper estimate, because the Fe(IV)═O $Por^{\bullet+}$ generated concomitantly with OCl^- (Scheme 1) would also likely lead to protein damage in the absence of a reductant.

The measurements examining heme and catalytic stability above (Figures 6 and 7) were conducted at a single pH (6.6). However, both the enzyme and the HOCl suicide reactant are known to undergo pH-dependent transitions. Second-order rate constants for the heme/NaOCl reaction (k) were therefore measured 1.5 pH units below and 0.5 pH unit above the $HOCl/OCl^-$ pK_a of 7.5 to assess which is the more likely reactive form. Heme decomposition was 1 order of magnitude faster in the presence of HOCl (pH 6; k = 0.13 M^{-1} s^{-1}) than in the presence of OCl^- (pH 8; k = 0.010 M^{-1} s^{-1}) (Figure S6 of the Supporting Information). However, the spin state of the heme also clearly undergoes changes from HS to LS within this pH range (Figures 3 and 4). Changes in the heme electronic state could therefore also contribute to these differences in reaction rate.

Measurement of MICs. *K. pneumoniae* exhibits substantial ClO_4^- and ClO_3^- tolerance under aerobic conditions, withstanding concentrations of ≥100 mM without significant growth defects. It is much more strongly affected by ClO_2^-. No growth was observed even at 20 mM $NaClO_2$, the lowest concentration tested. The mechanism of toxicity of ClO_2^- administered in the extracellular environment of bacteria has not been described. Lipid epoxidation, protein unfolding, and amino acid side chain modifications have all been observed in the presence of (H)OCl and could occur in the presence of ClO_2^-.[46] However, the $ClO_2^-/HClO_2$ pK_a (1.8) is significantly lower than that for OCl^-/HOCl.[47,48] Hence, chlorite and not hypochlorous acid is expected to predominate under biological conditions, where its negative charge should bar its passive entry into cells. Consistent with an expected extracytoplasmic mechanism of toxicity, ClO_2^- is equally toxic to cells possessing *Kp*Cld in the cytoplasm and those in which it is absent.

We hypothesized that ClO_3^- could be more toxic to *K. pneumoniae* that actively reducing NO_3^- is as a respiratory substrate. Consistent with that hypothesis, WT *K. pneumoniae* appears to become sensitized specifically to ClO_3^- (not ClO_4^- or ClO_2^-) under nitrate-respiring conditions (anaerobic, 50 mM KNO_3), exhibiting a MIC near 70 mM (Table 1). This shifts to 60 mM for the Δ*cld* mutant. These results suggest that *K. pneumoniae* metabolizes ClO_3^- under these conditions and that *Kp*Cld affords some protection against ClO_2^- produced endogenously from ClO_3^-. By contrast, ClO_4^- has no effect (up to 80 mM) on either the WT or Δ*cld* mutant strain of *K. pneumoniae*, under either aerobic or nitrate-respiring conditions. These results collectively suggest that ClO_4^- is not incorporated and/or metabolized by *K. pneumoniae*.

Table 1. Determination of ClO_3^- MICs for WT and Δ*cld* *K. pneumoniae* MGH under Aerobic and Nitrate-Respiring Conditions[a]

	WT		Δ*cld*	
[ClO_3^-] (mM)	aerobic	anaerobic	aerobic	anaerobic
30	++	++	++	++
40	++	++	++	+
50	++	++	++	+
60	++	+	++	−
70	++	+	++	−
80	++	−	++	−
100	++	−	++	−

[a]All cultures were grown in the presence of 50 mM added KNO_3. Legend: ++, robust growth; +, minor growth; −, no observable growth.

DISCUSSION

Chlorite dismutases are heme-binding proteins catalyzing steps in biological processes as divergent as perchlorate respiration and heme biosynthesis. Genetic and biological evidence has pointed toward a third, functionally distinct subgroup of the Cld family (Figure 2), members of which are found in diverse Gram-negative bacteria, including many obligate pathogens.[11,17] These bacteria are not known to respire (per)chlorate, nor do they lack any of the canonical genes required for making heme.[49] Their Cld proteins nonetheless share an almost identical active site with the respiration-associated Clds, though the overall monomer structure and oligomerization state differ. The biological role and distinct molecular features of this subgroup have been examined here, through biochemical investigation of *Kp*Cld and phenotypic characterization of the corresponding gene knockout in a pathogenic strain of *K. pneumoniae* (MGH 78578).

The Δ*cld* strain of *K. pneumoniae* had neither a growth defect nor any obvious sign of impaired heme metabolism. This contrasts sharply with the Δ*cld* strain of *S. aureus*, a slow-growing small colony variant with global deficiencies in its cellular heme levels.[14] We therefore investigated the hypothesis that the *cld* acts as an antioxidant toward chlorite or a related chlorine oxoanion. It was discovered that WT *K. pneumoniae* gains a noticeable growth advantage over its Δ*cld* counterpart in the presence of ClO_3^-. This advantage is observed

specifically under anaerobic, nitrate-respiring conditions (Table 1), even though *K. pneumoniae* does not have a dissimilatory reductase for either ClO_4^- or ClO_3^-, nor have these anions been shown to support anaerobic growth. It has been suggested that ClO_3^- might be taken up and metabolized by widespread bacterial nitrate-associated pathways.[50,51] Catalytic reduction of chlorate could be catalyzed by nitrate reductases because of the favorable reduction potential and kinetic lability of ClO_3^- relative to those of ClO_4^-; indeed, some nitrate reductases have been shown to accept chlorate as a substrate *in vitro*.[52,53] The product ClO_2^-, trapped inside the cell because of its charge, would be expected to quickly reach toxic levels if not enzymatically removed.[2] Hence, the Cld acts as an antioxidant against the ClO_2^- generated endogenously from ClO_3^-.

Such an antioxidant function, even in the absence of perchlorate or chlorate respiration, is consistent with both the catalytic properties of *Kp*Cld and the potent toxicity of ClO_2^-. Like superoxide dismutase or catalase, antioxidant enzymes against reduced oxygen species, *Kp*Cld is relatively fast [k_{cat} = $(1.9 \pm 0.2) \times 10^3$ s^{-1}; k_{cat}/K_M = $(2.5 \pm 0.4) \times 10^6$ M^{-1} s^{-1} (25 °C, pH 5)]. This suggests that it may effectively outcompete reactions between ClO_2^- and reactive intra- or extracellular components. Potential targets of ClO_2^--mediated damage are not as well characterized as those of HOCl;[46] however, ClO_2^- is known to act as an oxygen atom donor toward heme Fe(III) and reactive double bonds, as well as a source of highly reactive ClO_2 and HOCl.[42,43,54] These properties support its industrial use as a microbicide and bleach.[55]

*Kp*Cld's reactivity toward ClO_2^-, while rapid, is limited by the instability of the heme cofactor in the presence of its strongly oxidizing substrate. The heme spectrum and catalytic activity are completely eliminated by exposure to roughly 6000 equiv of ClO_2^- (Figure 6). The turnover number is enhanced by the inclusion of sacrifical reductants or chlorination traps in the reaction mixture, including DMSO, a reagent that combines rapidly and specifically with HOCl.[45] This strongly suggests that OCl^-, generated along with Fe^{IV}=O $Por^{\bullet+}$ from the heterolytic cleavage of the O−ClO^- bond (Scheme 1), is partially responsible for loss of the heme and its associated catalytic activity. This is consistent with recently reported results for a respiratory-type Cld from *N. defluvii* (discussed further below).[42]

The results also indirectly support the mechanism for O_2 generation proposed in Scheme 1, wherein the OCl^- leaving group recombines with the Fe(IV)=O $Por^{\bullet+}$ to produce O_2 and Cl^-. Kinetic sluggishness in the recombination would create the opportunity for release of OCl^-. Thus, the role of the arginine likely involves both steering the OCl^- leaving group and maintaining it in its more nucleophilic, anionic form, thereby mechanistically favoring the O−O bond forming reaction, as illustrated in Scheme 1. Evidence in support of this model is found in the sensitivity of Clds lacking the distal Arg to oxidative conditions. For example, the Cld from *S. aureus*, which contains a glutamine at the homologous position, undergoes complete beaching of the heme following exposure to only 5 equiv of ClO_2^-.[14] By the same token, substitution of the arginine in the *N. defluvii* Cld with a neutral residue strongly sensitizes its heme toward oxidant-mediated degradation.[42]

However, while HOCl is readily observed during chlorite turnover with *Kp*Cld, no MCD-trappable HOCl could be detected for *Da*Cld under conditions similar to those used here (Figure S7).[3] *Da*Cld is at the same time significantly less prone to catalytic inactivation (20000 turnovers vs 6000) and (H)OCl loss (Figure 6).[3,4] Hence, in spite of their shared O_2-evolving activity and conserved active site residues, including the distal Arg, the heme environment in dimeric *Kp*Cld and its pentameric *Da*Cld counterpart must be distinct in some ways.

The best insight into the nature of these distinctions comes from spectroscopic analysis of *Da*Cld and *Kp*Cld, which provides a nuanced view of the heme environment. First, it is clear from both EPR and rR that *Kp*Cld and *Da*Cld are different. The occurrence of a single axial ferric high-spin signal in the EPR spectrum of *Kp*Cld at pH <8.0 strongly contrasts with the case for *Da*Cld, which exhibits two rhombically distorted ferric EPR signals. In fact, among the few Clds for which the ferric EPR spectra have been reported so far, only *Nw*Cld shows the same axial signal as *Kp*Cld.[39] While the rR spectra of *Da*Cld and *Kp*Cld at pH 6 indicate high-spin heme, the enzymes differ in coordination state with *Da*Cld being 5c and *Kp*Cld having a significant population of 6c heme. Second, both EPR and rR spectra are consistent with water as the sixth ligand in *Kp*Cld at neutral pH. An increased level of access of water to the active site pocket in *Kp*Cld relative to *Da*Cld is suggested by the crystal structures of these two enzymes (Figure 8).

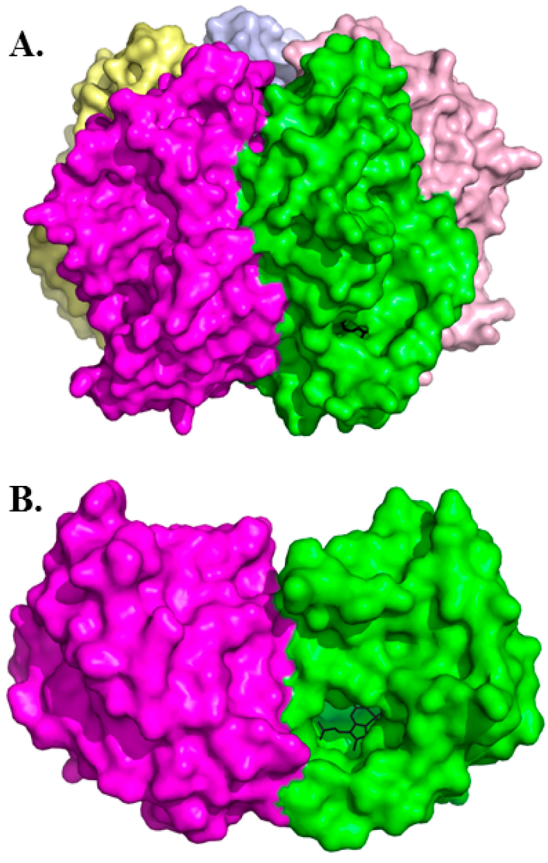

Figure 8. Surface rendering of *Nw*Cld and *Da*Cld in their expected native oligomerization states, showing differences in the entryway leading to the heme: (A) *Da*Cld pentamer (PDB entry 3Q08) and (B) *Nw*Cld dimer (PDB entry 3QPI). The monomers are rendered in different colors and the hemes in the green monomers shown as black sticks. The tunnel leading from the surface to the heme is more open in *Nw*Cld than in *Da*Cld. Figures generated by PyMol (www.pymol.com).

dx.doi.org/10.1021/bi501184c | *Biochemistry* 2015, 54, 434−446

Functionally, a more open catalytic pocket could explain the postulated lower fidelity in the recombination of Fe(IV)=O $Por^{\bullet+}$ with OCl^-, leading to a lower turnover number and a higher frequency of hypochlorous acid escape in *Kp*Cld (Figure 8). The Cld from *N. defluvii* shares spectral features with *Kp*Cld that are consistent with a more solvated distal pocket.[11] It likewise produces readily trappable HOCl during turnover with ClO_2^-,[42] and the EPR spectrum of its bound heme becomes undetectable after exposure to roughly 3000 equiv of ClO_2^-. Third, EPR characterization of mutants positioned within hydrogen bonding distance to the heme propionates (Y118F in *Da*Cld and Y62F *Kp*Cld) or within the second coordination sphere of the heme (W227 and W156 in *Da*Cld and Trp97 in *Kp*Cld) clearly indicates that both direct and indirect interactions influence the electronic structure of the heme. The fact that some of these (W227) are conserved only in the respiratory Clds suggests that they could contribute to the unique functional characteristics of those enzymes. Finally, the absence of second-sphere nitrogenous ligands that could explain the spin switch observed in frozen solution at pH 8 [85% conversion of the high-spin to low-spin ferric EPR signal (see Figure 4)] strongly argues for a repositioning of the guanidinium group of the distal side Arg in concert with formation of the Cld–OH complex and/or changes in hydrogen bonding interactions to the heme propionates. Effects of these kinds were reported for cytochrome *c* peroxidase, in relation to the formation of the ferryl–oxo intermediate.[56]

The relatively less robust *hemes* in *Kp*Cld and potentially other proteins in this subfamily are consistent with a biological role in providing intermittent protection against environmental ClO_3^-. The same may perhaps be true of the *N. defluvii* Cld that, though pentameric in structure like *Da*Cld and the other respiratory Clds (Figure 1, red), is extraordinary for being found within a species that is both non-perchlorate- or non-chlorate-respiring and phylogenetically distinct from any known respirers.[12] The gene's presence in this organism appears to be the result of lateral transfer; hence, as in *Kp*Cld, it may provide protection against environmental chlorate that is metabolized via nitrate-reducing pathways.

Of course, a chlorate-directed antioxidant role for *Kp*Cld and related enzymes (Figure 1, green) depends on the availability of chlorate in the natural environment. Perchlorate is used as an oxidant and propellant for rockets and fireworks, while chlorate is a common constituent of herbicides.[57] Because of their pervasive industrial use and the lack of a known geochemical mechanism for their formation, perchlorate and chlorate have long been thought to be largely unnatural in origin. However, the discovery of widespread perchlorate in pristine ground waters, ice cores, and undisturbed deserts prompted deeper investigation of its natural sources.[58−60] Potentially ancient atmospheric mechanisms for the generation of both perchlorate and chlorate are now favored on Earth and on Mars, where abundant perchlorate has been discovered.[61−66] Hence, Clds of the *Kp*Cld subtype may presently play an unaccounted-for role in Earth's chlorine cycle and could have done so for some time. It is likewise possible that they could serve a similar role against other halogen oxide species (e.g., iodate) that are especially abundant in nonterrestrial environments such as the open ocean.[67−69]

■ ASSOCIATED CONTENT

Supporting Information

Further description of *K. pneumoniae* mutant generation (Figure S1), rR spectra of ferrous *Kp*Cld (Figure S2), temperature dependence of the rR spectrum of *Kp*Cld (Figure S3), pH–rate profiles (Figure S4), NaOCl/*Kp*Cld titration data (Figure S5), reaction between NaOCl and *Kp*Cld monitored over time (Figure S6), and reaction between *Da*Cld and chlorite in the presence of MCD (Figure S7). This material is available free of charge via the Internet at http://pubs.acs.org.

■ AUTHOR INFORMATION

Corresponding Authors

*E-mail: jdubois@chemistry.montana.edu. Telephone: (406) 994-2844. Fax: (406) 994-5407.

*E-mail: gudrun.s.lukat-rodgers@ndsu.edu. Telephone: (701) 231-8834.

Funding

Support by National Institutes of Health Grants R01GM090260 (to J.L.D.), GM094039 (to G.S.L.-R.), and AI072719 (to K.R.R.) and by the CNRS (UMR 8221), CEA-Saclay, and the French Infrastructure for Integrated Structural Biology (FRISBI, ANR-10-INSB-05-01) (to A. I.) is gratefully acknowledged.

Notes

The authors declare no competing financial interest.

■ ACKNOWLEDGMENTS

Dr. Thomas Chen is thanked for the generation of the *Kp*Cld Y62F and W97F mutants, as well as preliminary work related to but eventually not published as part of this paper. Dr. Béatrice Blanc is thanked for generating the *Da*Cld W227F, W155F, and W156F mutants used in this work. Garrett Moraski is thanked for helpful discussions.

■ ABBREVIATIONS

Cld, chlorite dismutase; *Kp*Cld, *K. pneumoniae* Cld; *Da*Cld, *D. aromatica* Cld; *Nw*Cld, *Ni. winogradskyi* Cld; MIC, minimal inhibitory concentration; rR, resonance Raman; MCD, monochlorodimedone; EPR, electron paramagnetic resonance; WT, wild type; Por, porphyrin; Fe(IV)=O $Por^{\bullet+}$, ferryl–oxo porphyrin radical intermediate; HS, high-spin; LS, low-spin; 6cHS, six-coordinate, high-spin; 5cHS, five-coordinate, high-spin; 6cLS, six-coordinate, low-spin; PCR, polymerase chain reaction; PDB, Protein Data Bank.

■ REFERENCES

(1) Tagore, R., Crabtree, R. H., and Brudvig, G. W. (2008) Oxygen evolution catalysis by a dimanganese complex and its relation to photosynthetic water oxidation. *Inorg. Chem. 47*, 1815–1823.

(2) Coates, J. D., and Achenbach, L. A. (2004) Microbial perchlorate reduction: Rocket-fuelled metabolism. *Nat. Rev. Microbiol. 2*, 569–580.

(3) Streit, B. R., and DuBois, J. L. (2008) Chemical and steady state kinetic analyses of a heterologously expressed heme dependent chlorite dismutase. *Biochemistry 47*, 5271–5280.

(4) Lee, A. Q., Streit, B. R., Zdilla, M. J., Abu-Omar, M. M., and DuBois, J. L. (2008) Mechanism of and exquisite selectivity for O-O bond formation by the heme-dependent chlorite dismutase. *Proc. Natl. Acad. Sci. U.S.A. 105*, 15654–15659.

(5) Streit, B. R., Blanc, B., Lukat-Rodgers, G. S., Rodgers, K. R., and DuBois, J. L. (2010) How active-site protonation state influences the reactivity and ligation of the heme in chlorite dismutase. *J. Am. Chem. Soc. 132*, 5711–5724.

(6) Mayfield, J. A., Blanc, B., Rodgers, K. R., Lukat-Rodgers, G. S., and DuBois, J. L. (2013) Peroxidase-type reactions suggest a heterolytic/nucleophilic O-O joining mechanism in the heme-dependent chlorite dismutase. *Biochemistry 52*, 6982−6994.
(7) DuBois, J. L. (2014) *The Metal-Driven Biogeochemistry of Gaseous Compounds in the Environment* (Kroneck, P. M. H., and Sosa-Torres, M. E., Eds.) Chapter 8, Volume 15 of *Metal Ions in Life Sciences* (Sigel, A., Sigel, H., and Sigel, R.K.O., Eds.) Springer Science + Business Media B.V., Dordrecht, The Netherlands.
(8) Goblirsch, B. R., Streit, B. R., DuBois, J. L., and Wilmot, C. M. (2010) Structural features promoting dioxygen production by *Dechloromonas aromatica* chlorite dismutase. *JBIC, J. Biol. Inorg. Chem. 15*, 879−888.
(9) de Geus, D. C., Thomassen, E. A. J., Hagedoorn, P.-L., Pannu, N. S., van Duijn, E., and Abrahams, J. P. (2009) Crystal structure of chlorite dismutase, a detoxifying enzyme producing molecular oxygen. *J. Mol. Biol. 387*, 192−206.
(10) Kostan, J., Sjoeblom, B., Maixner, F., Mlynek, G., Furtmueller, P. G., Obinger, C., Wagner, M., Daims, H., and Djinovic-Carugo, K. (2010) Structural and functional characterisation of the chlorite dismutase from the nitrite-oxidizing bacterium "Candidatus *Nitrospira defluvii*": Identification of a catalytically important amino acid residue. *J. Struct. Biol. 172*, 331−342.
(11) Mlynek, G., Sjoeblom, B., Kostan, J., Fuereder, S., Maixner, F., Gysel, K., Furtmueller, P. G., Obinger, C., Wagner, M., Daims, H., and Djinovic-Carugo, K. (2011) Unexpected diversity of chlorite dismutases: A catalytically efficient dimeric enzyme from *Nitrobacter winogradsky*. *J. Bacteriol. 193*, 2408−2417.
(12) Maixner, F., Wagner, M., Luecker, S., Pelletier, E., Schmitz-Esser, S., Hace, K., Spieck, E., Konrat, R., Le Paslier, D., and Daims, H. (2008) Environmental genomics reveals a functional chlorite dismutase in the nitrite-oxidizing bacterium 'Candidatus *Nitrospira defluvii*'. *Environ. Microbiol. 10*, 3043−3056.
(13) Goblirsch, B., Kurker, R. C., Streit, B. R., Wilmot, C. M., and DuBois, J. L. (2011) Chlorite dismutases, DyPs, and EfeB: 3 Microbial heme enzyme families comprise the CDE structural superfamily. *J. Mol. Biol. 408*, 379−398.
(14) Mayfield, J. A., Hammer, N. D., Kurker, R. C., Chen, T. K., Ojha, S., Skaar, E. P., and DuBois, J. L. (2013) The chlorite dismutase (HemQ) from *Staphylococcus aureus* has a redox-sensitive heme and is associated with the small colony variant phenotype. *J. Biol. Chem. 288*, 23488−23504.
(15) Dailey, T. A., Boynton, T. O., Albetel, A.-N., Gerdes, S., Johnson, M. K., and Dailey, H. A. (2010) Discovery and characterization of HemQ an essential heme biosynthetic component. *J. Biol. Chem. 285*, 25978−25986.
(16) Blanc, B., Mayfield, J. A., McDonald, C. A., Lukat-Rodgers, G. S., Rodgers, K. R., and DuBois, J. L. (2012) Understanding how the distal environment directs reactivity in chlorite dismutase: Spectroscopy and reactivity of Arg183 mutants. *Biochemistry 51*, 1895−1910.
(17) Clark, I. C., Melnyk, R. A., Engelbrektson, A., and Coates, J. D. (2013) Structure and evolution of chlorate reduction composite transposons. *MBio 4*, e00379-13.
(18) Wisplinghoff, H., Bischoff, T., Tallent, S. M., Seifert, H., Wenzel, R. P., and Edmond, M. B. (2004) Nosocomial bloodstream infections in US hospitals: Analysis of 24,179 cases from a prospective nationwide surveillance study. *Clin. Infect. Dis. 39*, 309−317.
(19) Fabian, I., and Gordon, G. (1991) Complex-formation reactions of the chlorite ion. *Inorg. Chem. 30*, 3785−3787.
(20) Manoj, K. M., and Hager, L. P. (2006) A colorimetric method for detection and quantification of chlorinating activity of hemeperoxidases. *Anal. Biochem. 348*, 84−86.
(21) Jeffery, G. H., Bassett, J., Mendham, J., and Denney, R. C. (1989) *Vogel's Textbook of Quantitative Chemical Analysis*, Vol. 5th, Longman Scientific and Technical, New York.
(22) Zhang, Y., Jiang, X., Wang, Y., Li, G., Tian, Y., Liu, H., Ai, F., Ma, Y., Wang, B., Ruan, F., and Rajakumar, K. (2014) Contribution of β-lactamases and porin proteins OmpK35 and OmpK36 to carbapenem resistance in clinical isolates of KPC-2-producing *Klebsiella pneumoniae*. *Antimicrob. Agents Chemother. 58*, 1214−1217.
(23) Chaveroche, M., Ghigo, J., and d'Enfert, C. (2000) A rapid method for efficient gene replacement in the filamentous fungus *Aspergillus nidulans*. *Nucleic Acids Res. 28*, e97.
(24) Andrews, J. (2001) Determination of minimum inhibitory concentrations. *J. Antimicrob. Chemother. 48*, 5−16.
(25) Blanc, B., Rodgers, K. R., Lukat-Rodgers, G. S., and DuBois, J. L. (2013) Understanding the roles of strictly conserved tryptophan residues in O_2 producing chlorite dismutases. *Dalton Trans. 42*, 3156−3169.
(26) Berry, E. A., and Trumpower, B. L. (1987) Simultaneous determination of hemes a, b, and c from pyridine hemochrome spectra. *Anal. Biochem. 161*, 1−15.
(27) Silverman, R. B. (1995) Mechanism based enzyme inactivators. *Methods Enzymol. 249*, 240−283.
(28) Hagedoorn, P. L., de Geus, D. C., and Hagen, W. R. (2002) Spectroscopic characterization and ligand-binding properties of chlorite dismutase from the chlorate respiring bacterial strain GR-1. *Eur. J. Biochem. 269*, 4905−4911.
(29) Stenklo, K., Thorell, H. D., Bergius, H., Aasa, R., and Nilsson, T. (2001) Chlorite dismutase from *Ideonella dechloratans*. *JBIC, J. Biol. Inorg. Chem. 6*, 601−607.
(30) Bellelli, A., Antonini, G., Brunori, M., Springer, B. A., and Sligar, S. G. (1990) Transient spectroscopy of the reaction of cyanide with ferrous myoglobin: Effect of distal side residues. *J. Biol. Chem. 265*, 18898−18901.
(31) Chu, G. C., Tomita, T., Sonnichsen, F. D., Yoshida, T., and Ikeda-Saito, M. (1999) The heme complex of HmuO, a bacterial heme degradation enzyme from *Corynebacterium diphtheriae*: Structure of the catalytic site. *J. Biol. Chem. 274*, 24490−24496.
(32) Smulevich, G., Neri, F., Marzocchi, M., and Welinder, K. (1996) Versatility of heme coordination demonstrated in a fungal peroxidase. Absorption and resonance Raman studies of *Coprinus cinereus* peroxidase and the Asp245 → Asn mutant at various pH values. *Biochemistry 35*, 10576−10585.
(33) Asher, S. A., and Schuster, T. M. (1979) Resonance Raman examination of axial ligand bonding and spin-state equilibria in metmyoglobin hydroxide and other heme derivatives. *Biochemistry 18*, 5377−5387.
(34) Feis, A., Marzocchi, M. P., Paoli, M., and Smulevich, G. (1994) Spin state and axial ligand bonding in the hydroxide complexes of metmyoglobin, methemoglobin, and horseradish-peroxidase at room and low-temperatures. *Biochemistry 33*, 4577−4583.
(35) Yeh, S. R., Couture, M., Ouellet, Y., Guertin, M., and Rousseau, D. L. (2000) A cooperative oxygen finding hemoglobin from *Mycobacterium tuberculosis*: Stabilization of heme ligands by a distal tyrosine residue. *J. Biol. Chem. 275*, 1679−1684.
(36) Lukat-Rodgers, G. S., and Rodgers, K. R. (1998) Spin-state equilibria and axial ligand bonding in FixL hydroxide: A resonance Raman study. *JBIC, J. Biol. Inorg. Chem. 3*, 274−281.
(37) Colin, J., Wiseman, B., Switala, J., Loewen, P., and Ivancich, A. (2009) Distinct role of specific tryptophans in facilitating electron transfer or as [Fe(IV)═O $Trp^{\bullet}$] intermediates in the peroxidase reaction of *Bulkholderia pseudomallei* catalase-peroxidase: A multifrequency EPR spectroscopy investigation. *J. Am. Chem. Soc. 131*, 8557−8563.
(38) Deemagarn, T., Wiseman, B., Carpena, X., Ivancich, A., Fita, I., and Loewen, P. (2007) Two alternative substrate paths for compound I formation and reduction in catalase-peroxidase KatG from *Burkholderia pseudomallei*. *Proteins: Struct., Funct., Bioinf. 66*, 219−228.
(39) Singh, R., Switala, J., Loewen, P. C., and Ivancich, A. (2007) Two [Fe(IV)═O Trp*] intermediates in *M. tuberculosis* catalase-peroxidase discriminated by multifrequency (9−285 GHz) EPR spectroscopy: Reactivity toward isoniazid. *J. Am. Chem. Soc. 129*, 15954−15963.
(40) Hofbauer, S., Bellei, M., Sundermann, A., Pirker, K., Hagmuller, A., Mlynek, G., Kostan, J., Daims, H., Furtmuller, P., Djinovic-Carugo, K., Oostenbrink, C., Battistuzzi, G., and Obinger, C. (2012) Redox

thermodynamics of high-spin and low-spin forms of chlorite dismutases with diverse subunit and oligomeric structures. *Biochemistry 51*, 9501−9512.
(41) Silverman, R. B. (1988) *Mechanism-Based Enzyme Inactivation: Chemistry and Enzymology*, Vol. *I*, CRC Press, Inc., Boca Raton, FL.
(42) Hofbauer, S., Gruber, C., Pirker, K., Sundermann, A., Schaffner, I., Jakopitsch, C., Oostenbrink, C., Furtmuller, P., and Obinger, C. (2014) Transiently produced hypochlorite is responsible for the irreversible inhibition of chlorite dismutase. *Biochemistry 53*, 3145−3157.
(43) Jakopitsch, C., Pirker, K., Flemmig, J., Hofbauer, S., Schlorke, D., Furtmuller, P., Arnhold, J., and Obinger, C. (2014) Mechanism of reaction of chlorite with mammalian heme peroxidases. *J. Inorg. Biochem. 135*, 10−19.
(44) Shahangian, S., and Hager, L. P. (1981) The reaction of chloroperoxidase with chlorite and chlorine dioxide. *J. Biol. Chem. 256*, 6034−6040.
(45) Lehtimaa, T., Kuitunen, S., Tarvo, V., and Vuorinen, T. (2010) Kinetics of aldehyde oxidation by chlorous acid. *Ind. Eng. Chem. Res. 49*, 2688−2693.
(46) Winter, J., Ilbert, M., Graf, P. C. F., Oezcelik, D., and Jakob, U. (2008) Bleach activates a redox-regulated chaperone by oxidative protein unfolding. *Cell 135*, 691−701.
(47) Shriver, D., and Atkins, P. (2009) *Inorganic Chemistry*, 5th ed., pp 830, W. H. Freeman, New York.
(48) Taylor, J. B., and Wohlers, D. W. (2004) Toxicological profile for chlorine dioxide and chlorite. U.S. Environmental Protection Agency, Washington, DC.
(49) Panek, H., and O'Brian, M. R. (2002) A whole genome view of prokaryotic haem biosynthesis. *Microbiology (Reading, U.K.) 148*, 2273−2282.
(50) Parsonage, D., and Ferguson, S. (1983) Reassessment of pathways of electron flow to nitrate reductase that are coupled to energy-conservation in *Paracoccus denitrificans*. *FEBS Lett. 153*, 108−112.
(51) Stewart, V. (1988) Nitrate respiration in relation to facultative metabolism in enterobacteria. *Microbiol. Rev. 52*, 190−232.
(52) Yoshimatsu, K., Sakurai, T., and Fujiwara, T. (2000) Purification and characterization of dissimilatory nitrate reductase from a denitrifying halophilic archaeon, *Haloarcula marismortui*. *FEBS Lett. 470*, 216−220.
(53) Afshar, S., Johnson, E., de Vries, S., and Schroder, I. (2001) Properties of a thermostable nitrate reductase from the hyperthermophilic archaeon *Pyrobaculum aerophilum*. *J. Bacteriol. 183*, 5491−5495.
(54) Jakopitsch, C., Spalteholz, H., Fürtmuller, P. G., Arnhold, J., and Obinger, C. (2008) Mechanism of reaction of horseradish peroxidase with chlorite and chlorine dioxide. *J. Inorg. Biochem. 102*, 293−302.
(55) Richardson, S. D. (2003) Disinfection by-products and other emerging contaminants in drinking water. *Trends Anal. Chem. 22*, 666−684.
(56) Bonagura, C. A., Bhaskar, B., Shimizu, H., Li, H. Y., Sundaramoorthy, M., McRee, D. E., Goodin, D. B., and Poulos, T. L. (2003) High-resolution crystal structures and spectroscopy of native and compound I cytochrome c peroxidase. *Biochemistry 42*, 5600−5608.
(57) Urbansky, E. T. (1998) Perchlorate chemistry: Implications for analysis and remediation. *Biorem. J. 2*, 81−95.
(58) Rao, B., Anderson, T., Orris, G., Rainwater, K., Rajagopalan, S., Sandvig, R., Scanlon, B., Stonestrom, D., Walvoord, M., and Jackson, W. (2007) Widespread natural perchlorate in unsaturated zones of the southwest United States. *Environ. Sci. Technol. 41*, 4522−4528.
(59) Scanlon, B. R., Reedy, R. C., Jackson, W. A., and Rao, B. (2008) Mobilization of naturally occurring perchlorate related to land-use change in the southern high plains, Texas. *Environ. Sci. Technol. 42*, 8648−8653.
(60) Furdui, V. I., and Tomassini, F. (2010) Trends and sources of perchlorate in arctic snow. *Environ. Sci. Technol. 44*, 588−592.
(61) Rao, B. A., Wake, C. P., Anderson, T., and Jackson, W. A. (2012) Perchlorate depositional history as recorded in North American ice cores from the Eclipse Icefield, Canada, and the Upper Fremont Glacier, USA. *Water, Air, Soil Pollut. 223*, 181−188.
(62) Rao, B., Mohan, S., Neuber, A., and Jackson, W. A. (2012) Production of perchlorate by laboratory simulated lightning process. *Water, Air, Soil Pollut. 223*, 275−287.
(63) Catling, D., Claire, M., Zahnle, K., Quinn, R., Clark, B., Hecht, M., and Kounaves, S. (2010) Atmospheric origins of perchlorate on Mars and in the Atacama. *J. Geophys. Res.: Planets 115*, E00E11.
(64) Kounaves, S., Carrier, B., O'Neil, G., Stroble, S., and Claire, M. (2014) Evidence of martian perchlorate, chlorate, and nitrate in Mars meteorite EETA79001: Implications for oxidants and organics. *Icarus 229*, 206−213.
(65) Hecht, M. H., Kounaves, S. P., Quinn, R. C., West, S. J., Young, S. M. M., Ming, D. W., Catling, D. C., Clark, B. C., Boynton, W. V., Hoffman, J., DeFlores, L. P., Gospodinova, K., Kapit, J., and Smith, P. H. (2009) Detection of perchlorate and the soluble chemistry of Martian soil at the Phoenix Lander site. *Science 325*, 64−67.
(66) Balaji Rao, B. R., Hatzinger, P. B., Bohlke, J. K., Sturchio, N. C., Andraski, B. J., Eckardt, F. D., and Jackson, W. A. (2010) Natural chlorate in the environment: Application of a new IC-ESI/MS/MS method with a $Cl^{18}O_3$-internal standard. *Environ. Sci. Technol. 44*, 8429−8434.
(67) Lu, Z., Jenkyns, H., and Rickaby, R. (2010) Iodine to calcium ratios in marine carbonate as a paleo-redox proxy during oceanic anoxic events. *Geology 38*, 1107−1110.
(68) Xu, S., Xie, Z., Li, B., Liu, W., Sun, L., Kang, H., Yang, H., and Zhang, P. (2010) Iodine speciation in marine aerosols along a 15000-km round-trip cruise path from Shanghai, China, to the Arctic Ocean. *Environ. Chem. 7*, 406−412.
(69) Tamura, K., Stecher, G., Peterson, D., Filipski, A., and Kumar, S. (2013) MEGA6: Molecular Evolutionary Genetics Analysis version 6.0. *Mol. Biol. Evol. 30*, 2725−2729.
(70) Le, S. Q., Dang, C. C., and Gascuel, O. (2012) Modeling protein evolution with several amino acid replacement matrices depending on site rates. *Mol. Biol. Evol. 29*, 2921−2936.
(71) Melnyk, R. A., Engelbrektson, A., Clark, I. C., Carlson, H. K., Byrne-Bailey, K., and Coates, J. D. (2011) Identification of a perchlorate reduction genomic island with novel regulatory and metabolic genes. *Appl. Environ. Microbiol. 77*, 7401−7404.